Proc. Natl. Acad. Sci. USA
Vol. 87, pp. 4149–4153, June 1990
Medical Sciences

Distribution of trace levels of therapeutic gallium in bone as mapped by synchrotron x-ray microscopy

R. S. BOCKMAN*†, M. A. REPO*, R. P. WARRELL, JR.*, J. G. POUNDS‡, G. SCHIDLOVSKY‡, B. M. GORDON‡, AND K. W. JONES‡

*Cornell University Medical College, The Hospital for Special Surgery and Memorial Sloan–Kettering Cancer Center, New York, NY 10021; and ‡Brookhaven National Laboratory, Upton, NY 11973

Communicated by Eugene P. Cronkite, January 18, 1990

ABSTRACT **Gallium nitrate, a drug that inhibits calcium release from bone, has been proven a safe and effective treatment for the accelerated bone resorption associated with cancer. Though bone is a target organ for gallium, the kinetics, sites, and effects of gallium accumulation in bone are not known. We have used synchrotron x-ray microscopy to map the distribution of trace levels of gallium in bone. After short-term *in vivo* administration of gallium nitrate to rats, trace (nanogram) amounts of gallium preferentially localized to the metabolically active regions in the metaphysis as well as the endosteal and periosteal surfaces of diaphyseal bone, regions where new bone formation and modeling were occurring. The amounts measured were well below the levels known to be cytotoxic. Iron and zinc, trace elements normally found in bone, were decreased in amount after *in vivo* administration of gallium. These studies represent a first step toward understanding the mechanism(s) of action of gallium in bone by suggesting the possible cellular, structural, and elemental "targets" of gallium.**

Gallium, a group IIIa transition element, has been used to safely and effectively treat life-threatening hypercalcemia in cancer patients (1–6). Gallium is thought to accumulate within bone (7–13) and act to reduce calcium loss by inhibiting bone resorption without causing apparent damage to bone cells (8). The mechanism of action of gallium is not known. We require, as a first step, knowledge of exactly where within bone this therapeutic agent accumulates. We have used synchrotron radiation-induced x-ray emission to quantitatively map the microscopic distribution of gallium in sections of growing rat bones and to study gallium's effects on other trace elements. The synchrotron radiation source provides an intense flux of collimated and polarized x-rays; this dense flux is needed to detect trace elements in the bone matrix with a high degree of spatial resolution.

METHODS

Female Sprague–Dawley rats (6 weeks of age, 120 g) were injected intraperitoneally with gallium nitrate (0, 2.5, or 25 mg/kg per rat) every other day for 14 days. Each rat received a total of 0, 0.6, or 6 mg of elemental gallium [doses that were similar to those used in the human studies (1–6)]; no differences in size, weight, or general condition were noted in the three groups of animals at the end of the treatment schedule. One hour after the last injection, the animals were sacrificed. The tibial bones were removed, cleaned of adventitial tissue, and rapidly frozen in Tissue.Tek II (Lab-Tek) over dry ice or placed in buffered formalin, dehydrated in alcohol, and eventually embedded in methacrylate. The frozen bones were longitudinally sectioned on a cryostat, placed onto 7.3-μm polyimide support film mounted in cardboard slide mounts, and then lyophilized for 18–24 hr. The bones embedded in methacrylate were sectioned at 8 μm and then mounted onto cardboard slide mounts. Alternate sections were placed on glass slides and then stained for histologic analysis.

Fetal (19–20 day) rat bones, freed of all adventitial tissue, as described (1), were bathed in medium (BGJ; GIBCO) containing 25 μM gallium for 48 hr. The bones were then thoroughly rinsed with fresh medium and buffered saline. The bones were frozen in Tissue.Tek, sectioned, and then studied by synchrotron x-ray microscopy.

X-ray microscopy studies were carried out at the National Synchrotron Light Source X-26 x-ray microscopy (XRM) facility (14–16) at the Brookhaven National Laboratory (Upton, NY). This synchrotron radiation source provides the necessary flux of collimated and polarized x-rays that are used to detect trace elements of high atomic number in biologic samples. The nondecalcified bone sections were placed on a computer-controlled stage capable of moving the sample in 1-μm increments in three dimensions. An energy dispersive Si(Li) detector, placed at 90° to the incident beam to reduce the magnitude of Rayleigh and Compton scattering, was used to detect emitted photons from the radiated sample. The exciting x-ray beam from the synchrotron ring passed through two 25.4-μm beryllium windows. Most low-energy photons (<2.5 keV; 1 eV = 1.602×10^{-19} J) in the primary beam were absorbed by the beryllium windows and a 250-μm aluminum absorber. A 225-μm polyimide absorber, placed at the detector, reduced the intensity of the calcium K x-rays that were emitted from the bone specimens. Each bone section was systematically scanned by using a beam aperture that was 40 × 40 or 100 × 100 μm. The position of the beam on the sample target was monitored with a stereo microscope. Emission spectra were stored and analyzed by using a Digital Equipment Corporation MicroVax II computer and a Nuclear Data Corporation (ND9900) data acquisition system (14–16).

In each bone section, the x-ray emission peaks from the high atomic number elements were identified, and the area under each peak was calculated. An efficiency curve was determined for each run by using a standard bone section, and from that curve, the elemental concentrations of the trace elements for that run were calculated. To eliminate errors due to variations in sample thickness or the amount of bone mineral under the beam, the data were usually normalized to calcium content, and the data were expressed as the weight ratio of the trace element to calcium.

The proximal tibiae or distal femurs were selected for their simplicity of structure; the two major regions studied were the metaphysis and diaphysis (Fig. 1). The metaphysis, at the

The publication costs of this article were defrayed in part by page charge payment. This article must therefore be hereby marked "*advertisement*" in accordance with 18 U.S.C. §1734 solely to indicate this fact.

Abbreviation: XRM, x-ray microscopy.

†To whom reprint requests should be addressed at: The Hospital for Special Surgery, 535 70th Street, New York, NY 10021.

proximal end of the tibia, begins below the epiphysis. In this region of the rat tibia, linear bone growth produces a newly mineralized metaphyseal region every 2 weeks (17). The diaphysis or shaft region between the metaphyseal ends of the bone is made up of mature compact bone. The diaphysis grows circumferentially (is modeled slowly throughout the life of the rat) with a net accretion (addition of bone) at the outer (periosteal) surface and a net resorption at the inner (endosteal) surface.

RESULTS

A typical synchrotron radiation-induced x-ray emission spectrum from a single 100- × 100-μm region in the proximal metaphysis of a 12-μm-thick, nondecalcified cryostat-prepared bone section is shown in Fig. 2. The characteristic K lines from gallium and other trace elements (iron, copper, zinc, and strontium) as well as the major element, calcium, present in the sample were clearly identified by their distinctive Kα and Kβ emission energies (3.69 and 4.012 keV for calcium; 9.24 and 10.26 keV for gallium). The weight ratios for each element measured in the different bone regions are summarized in Table 1. Trace element levels in a control bone were compared to those from an animal that had received 0.6 mg of elemental gallium. No evidence for gallium K x-rays was found in any of the bones of control animals (i.e., those not treated with gallium), confirming that gallium is not normally found as a trace element in rat bones. For the gallium-treated rats, significantly more gallium was measured in the metaphyseal bone region, a result previously demonstrated by studies of pooled bone samples analyzed by atomic absorption (11, 12). Higher levels of the trace elements iron, copper, and zinc were found in the metaphyseal regions than in the diaphysis. No differences in the strontium-to-calcium ratios were noted in the different bone regions. Significantly less iron content (relative to control values) was found in the metaphysis and diaphysis of tibiae from gallium-treated rats. A small but significant decrease in zinc content was observed in the metaphysis but not the diaphysis of test animals.

The microscopic distribution of gallium in the different bone regions was mapped by XRM scanning of specific areas on the bone sections. In each 40- × 40-μm or 100- × 100-μm pixel, the intensity of Kα of emissions, calcium, gallium, iron, zinc, copper, and strontium was determined. Histograms or pseudocolor maps were constructed in order to compare the distribution pattern of the selected trace elements. A typical histogram of gallium distribution in the proximal tibia of an adult rat that received a total of 0.6 mg of elemental gallium over 2 weeks is illustrated in Fig. 3 along with a low-magnification scanning electron micrograph of the bone section. The regions with the greatest gallium content were the proximal central metaphyseal region and the inner (endosteal) and outer (periosteal) aspects of the diaphysis.

We next quantified gallium and calcium content in specific regions of adult rat bones. Systematic linear scans performed longitudinally down the central metaphysis (≈800 μm) and transversely across the cortical bone of the diaphysis (≈500 μm) were compared (Fig. 4). The gallium-to-calcium ratios in the metaphysis were significantly greater than those in the cortical bone due to the higher gallium and lower calcium concentrations in the metaphysis compared to the diaphysis (see Table 1). A small decrease in the gallium-to-calcium ratio was noted as the beam scanned longitudinally from proximal to distal portions of the metaphysis (Fig. 4). This decrease was minor in comparison to the precipitous decrease in the gallium-to-calcium ratios observed in the midcortical region between the endosteal and periosteal surfaces of the diaphysis. XRM scans taken transversely across the cortical bone (from endosteal surface to periosteal surface) showed that the calcium content across the cortex was constant and significantly greater than the calcium content measured in the metaphysis (Table 1). The gallium content in the cortical bone was very low in the midcortical region, accounting for the precipitous trough in the gallium-to-calcium ratio (Fig. 4).

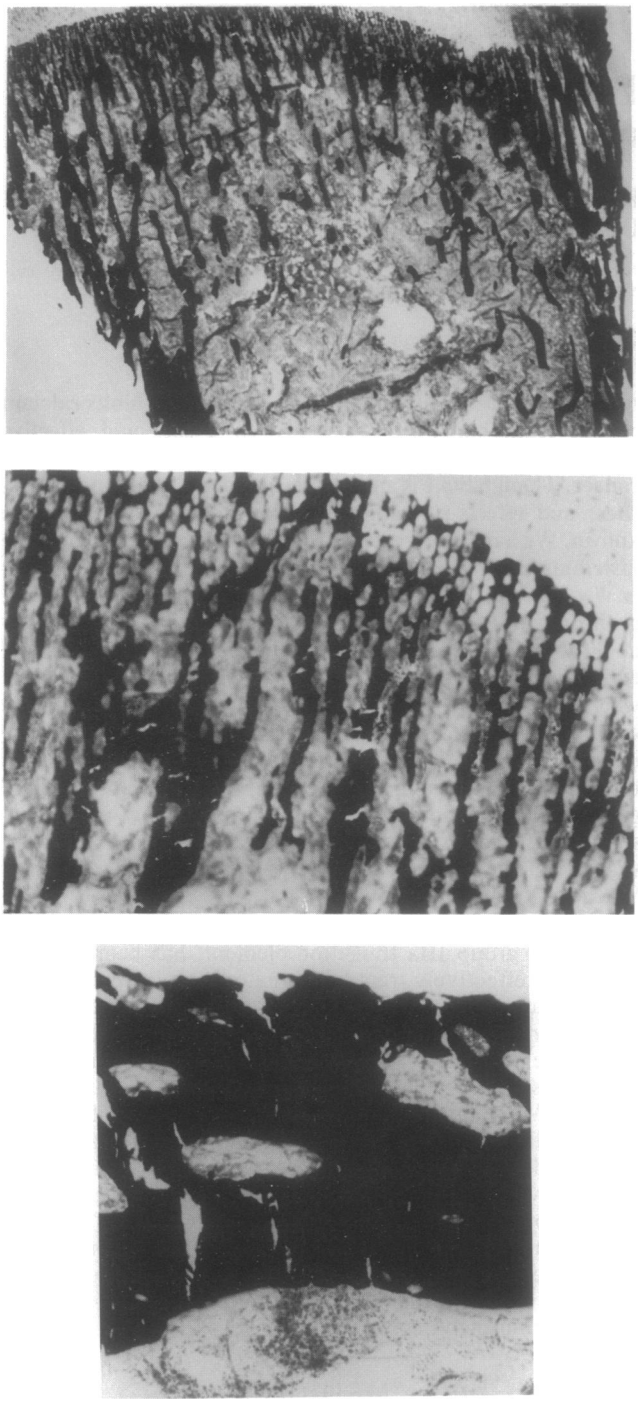

FIG. 1. Photomicrographs of a rat tibial bone that was embedded in methacrylate and stained with the Von Kossa stain. (*Top*) The proximal tibia just below the epiphyseal cartilage is shown; it contains the metaphysis as well as a portion of the diaphysis (×10). The regions scanned for the XRM studies include a two-dimensional scan of the entire proximal tibia (see Fig. 3), a linear scan of a single column of calcified matrix from the epiphyseal cartilage to its termination at the marrow cavity (*Middle*), and a section of diaphyseal bone (*Bottom*). Data from the linear scans are illustrated in Fig. 4. (*Middle*, ×20; *Bottom*, ×50.)

Fetal rat bones exposed to 25 μM gallium *in vitro* had readily measurable levels of gallium. No gallium could be found in the untreated bones. The pattern of gallium distri-

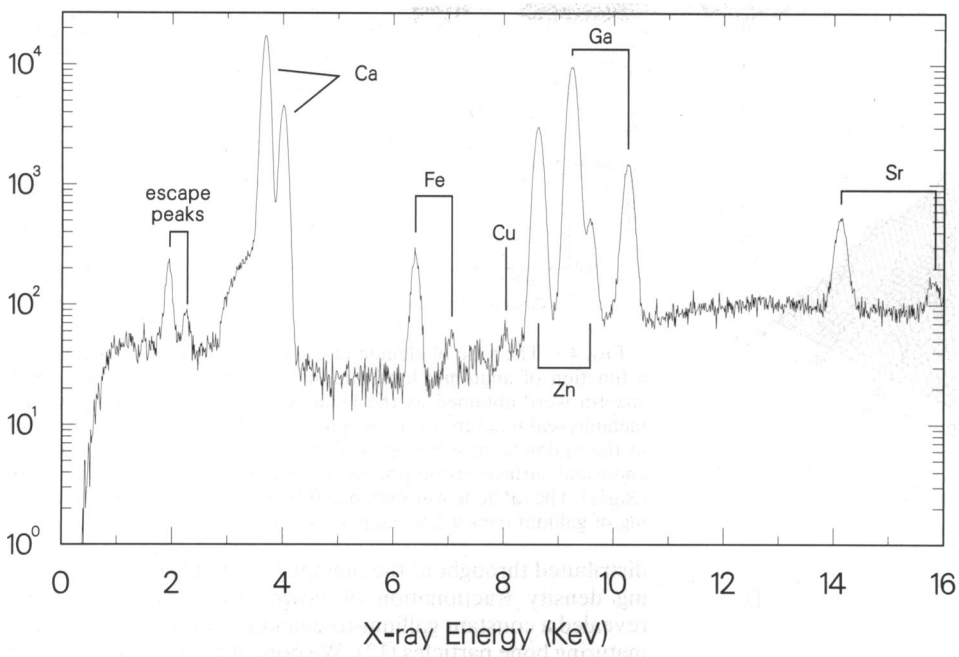

FIG. 2. Typical x-ray spectrum obtained from a 100- × 100-μm area of a 12-μm-thick bone section from the tibia of a rat that received 0.6 mg of elemental gallium over a 2-week period. The emission peaks (K lines) for the various elements in the proximal metaphysis are illustrated.

bution in fetal bones exposed to gallium (25 μM) *in vitro* for 48 hr was examined for comparison with the adult bones. In the fetal rat bones, gallium preferentially accumulated in the sites that had the greatest calcium content, notably in the newly calcified trabecular and cortical regions of the forming diaphysis. Neither gallium or calcium were present to any significant extent in the cartilaginous ends of these fetal bones (Fig. 5). In these fetal bones, new bone formation (mineralization) was occurring throughout the forming diaphysis; gallium was found to be evenly distributed along with calcium in these calcifying regions. The concentrations of trace elements, iron, copper, and zinc, were considerably lower than the concentrations measured in the corresponding regions of adult bones. The effect of gallium exposure on these trace elements could not be determined. Direct exposure of mineralizing tissue to gallium nitrate produced higher ratios of gallium to calcium in bone compared to the ratios in adult bones exposed to gallium *in vivo*.

DISCUSSION

The current synchrotron XRM studies illustrate the power of this technology in providing microscopic spatial resolution and quantification of trace (high atomic number) elements in bone. Our results stand in contrast to electron or ion probe microscopy attempts that have failed to demonstrate any significant gallium concentration in bone even after doses much higher than those used here were tested (7). Bone

Table 1. Weight ratios of trace elements to calcium in bone

Sample	Trace element-to-calcium ratio × 10^3				
	Iron	Copper	Zinc	Gallium	Strontium
			Adult rat*		
Metaphysis					
Control	0.79 ± 0.16	0.016 ± 0.004	0.84 ± 0.10	ND	0.20 ± 0.01
Gallium	0.42 ± 0.05†	0.026 ± 0.007	0.61 ± 0.03‡	0.35 ± 0.02	0.18 ± 0.01
Diaphysis					
Control	0.27 ± 0.04	ND	0.37 ± 0.05	ND	0.26 ± 0.02
Gallium	0.07 ± 0.02§	ND	0.49 ± 0.05	0.10 ± 0.07¶	0.21 ± 0.01
			Fetal rat‖		
Control	0.06	ND	0.06	ND	ND
Gallium	0.09 ± 0.03	ND	0.05 ± 0.01	1.92 ± 0.56	0.01 ± 0.001

The data are represented as the weight ratio of each element normalized to calcium content in the beam field (calculated volume in the beam was 3×10^{-5} μl). For readability, the ratios have been multiplied by 1000. Simultaneous measurements were made for each element, in the same bone volume and location, which automatically normalizes the data for section-to-section variability with regard to specimen thickness. Each data point is the mean ± SEM of 6–12 separate measurements. ND, Not detectable.

*The concentration of calcium calculated by using known bone mineral standards was 0.13 ± 0.03 and 0.13 ± 0.02 g/ml in the metaphyses of control and gallium-treated rats, respectively. The calcium concentration measured in the diaphyseal samples varied between 0.27 and 0.37 g/ml and was significantly greater than that of the metaphysis ($P < 0.001$). Except for strontium, trace element concentrations in the diaphysis were significantly ($P < 0.001$) lower than the levels in the metaphysis.

†Differs from control, $P < 0.02$ (the student t test of means).

‡Differs from control, $P < 0.008$.

§Differs from control, $P < 0.0005$.

¶Differs from metaphysis, $P < 0.01$.

‖Measurements were made over regions containing bone mineral and include trabecular and cortical bone. Bones were exposed to 25 μM gallium nitrate for 48 hr.

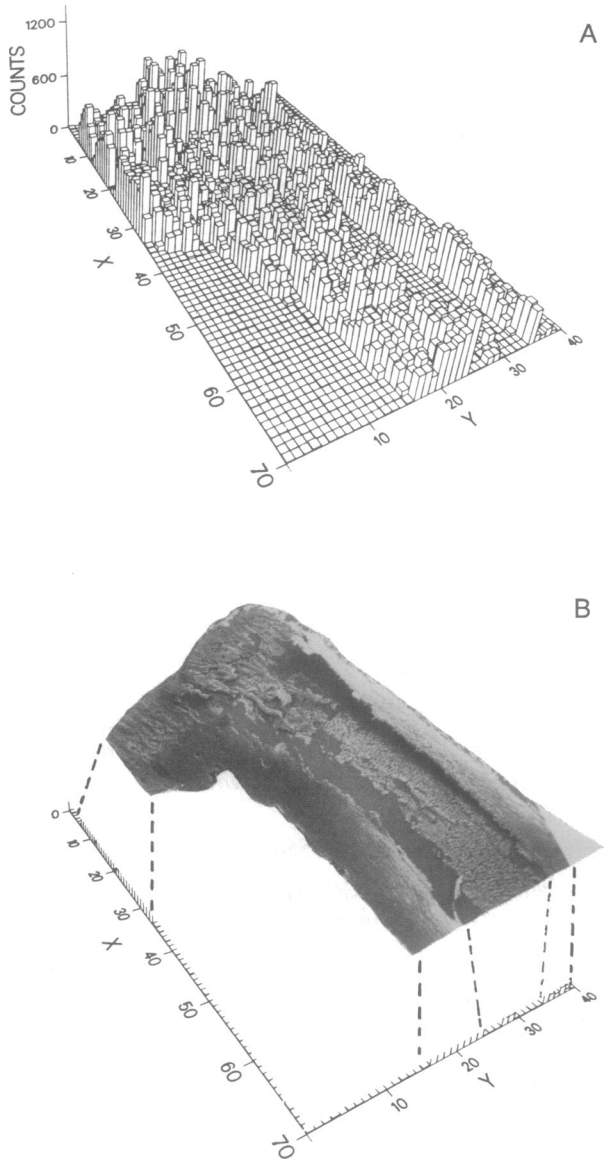

FIG. 3. (*A*) Histogram illustrating the distribution of gallium in the proximal metaphysis and a portion of the diaphysis of the tibia as illustrated in Fig. 1. The histogram was constructed from sequential spectra obtained from 100- × 100-μm areas on the tibial bone section. (*B*) A low-magnification scanning electron micrograph of the proximal tibia prepared from a dehydrated cryostat prepared bone section is presented for comparison.

biopsy performed in patients with Paget's disease who received radioactive gallium-67 citrate showed that gallium accumulated over the nuclei of osteoclasts (13). The current studies do not achieve the resolution of autoradiography with electron microscopy. Nonetheless, from the XRM it is evident that, after treatment with therapeutic levels of gallium, the agent preferentially localizes to metabolically active regions of bone where both resorption and formation (modeling) are occurring. These regions contain osteoclasts and osteoblasts that are actively modeling bone. The XRM studies document that the concentrations of gallium accumulating in these "target" regions are well below known toxic levels (8).

During the 2-week period in which the rats were studied, an entirely new metaphysis was formed due to longitudinal bone growth. One would anticipate that all mineralizing particles in the newly forming metaphyses had been equally exposed to gallium administered over the same time period. Our XRM scans have shown that gallium was uniformly

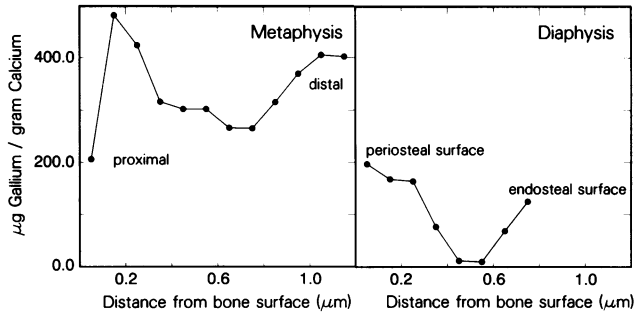

FIG. 4. The ratio of elemental gallium to calcium is illustrated as a function of anatomic localization in adult rat tibial bone. XRM spectra were obtained as the beam scanned from the epiphyseal–metaphyseal juncture to the beginning of the marrow space (distal) in the midmetaphyseal region (*Left*) or from the periosteal to the endosteal surface of the proximal portion of the diaphyseal cortex (*Right*). The rat bone was obtained from an adult rat that received 0.6 mg of gallium over a 2-week period as described in Fig. 2.

distributed throughout the metaphysis. Earlier studies utilizing density fractionation of powdered metaphyseal bone revealed a constant gallium-to-calcium ratio in immature and maturing bone particles (12). We conclude that newly formed as well as growing bone particles in the metaphysis accumulate gallium. Since linear bone growth is not different in rats treated with gallium compared to controls, gallium accumulation does not appear to inhibit bone growth (R. Donnelly, R.S.B., and A. Boskey, unpublished results).

We observed that the gallium and calcium content rose slightly in the midregion of the metaphysis, the same region where a slight depression in the gallium-to-calcium ratio was noted (Fig. 4 *Left*). This small change in the gallium-to-calcium ratio resulted from a relative increase in calcium

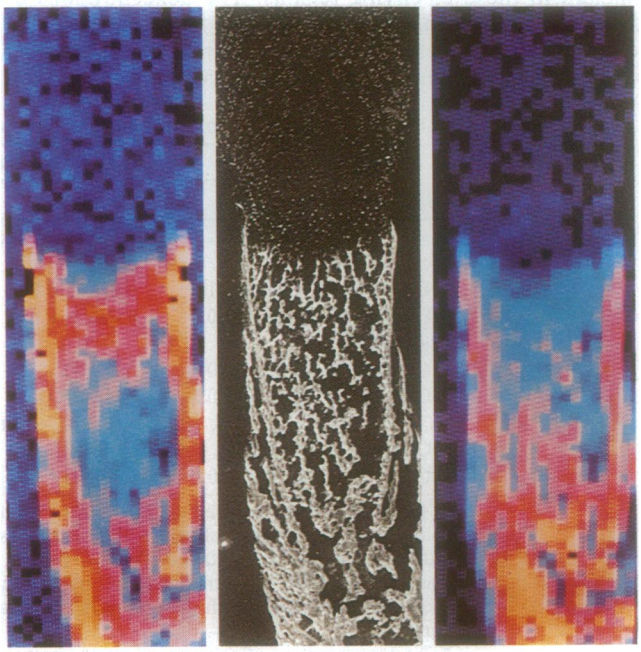

FIG. 5. Pseudocolor maps illustrate the distribution of gallium (*Left*) and calcium (*Right*) in a fetal rat ulna bone that had been exposed to gallium (25 μM) in the culture medium for 48 hr. Yellow indicates bone regions having the greatest concentration of the study element, and blue indicates the regions having the lowest concentration. (*Center*) A low-magnification scanning electron micrograph of the study bone illustrates the metaphyseal and diaphyseal portions composed of calcifying cortical and trabecular bone as well as the noncalcified, distal cartilaginous end, which accumulates little gallium compared to the calcified portions.

content compared to gallium within a region distal to the cartilage (epiphyseal)–metaphyseal juncture. In a previously reported histomorphometric analysis of the rat tibial metaphysis, a peak in bone mineral (calcium) content was found several hundred microns distal to the cartilage–metaphyseal junction (17), the same region represented by the depression in Fig. 4 *Left*. This region includes calcifying cartilage as well as newly calcifying trabeculae (17). The additional data provided by the XRM scans suggest that calcium accretion may have exceeded gallium accumulation in this particular region. Preliminary studies in healing rachitic bones suggest that calcium accretion can outstrip gallium accumulation when rapid mineralization is occurring (R. Donnelly, R.S.B., and A. Boskey, unpublished results).

Linear XRM scans across cortical bone confirmed that a uniform concentration of calcium existed across the region. Gallium concentration, however, reached a nadir in the midcortical region as illustrated in Fig. 4 *Right*. We have also studied diaphyseal bone powder by densitometric analysis (12). Such bone particles were highly mineralized and composed of mature hydroxyapatite (12). Although the cortical bone was relatively homogeneous with regard to calcium content, the most mature particles (those with the greatest density and slowest turnover thought to come from the midcortical region) had the lowest gallium content (12). Cortical bone is modeled slowly; the midcortical region is least accessible to metabolically active bone cells and has the slowest turnover (17). Decreased gallium accumulation in the midcortical region is most likely a consequence of the low metabolic activity of this bone region. Passive diffusion of gallium does not seem to occur readily.

To summarize, the greatest concentrations of gallium were found in the metaphysis as well as on the endosteal and periosteal surfaces of cortical bone. The lowest concentrations of gallium were observed in the relatively acellular, metabolically inactive midcortical regions. We conclude from these studies that gallium preferentially localized to the metabolically active regions where bone modeling (resorption and formation, including mineralization) were occurring. This phenomenon was also evident in the fetal bones where gallium and calcium preferentially coaccumulated in the region where active mineralization had been occurring. The amount of gallium that accumulated after *in vitro* exposure of bone explants was much greater than the levels achieved after *in vivo* administration (Table 1; refs. 11 and 12). It would appear that newly forming bone matrix has a large capacity to accumulate gallium. However, toxic levels are not reached following *in vivo* administration of therapeutic doses even after 8–10 weeks of continuous administration due to the fact that gallium accumulation in bone is reversible and the amounts reaching the bone are limited by the dose given (12).

Our findings with gallium contrast strikingly with the published data for aluminum, another group IIIa metal that has had wide therapeutic use in antacids. Following aluminum administration to rats at doses similar to the gallium doses used in the current study, a dense band of aluminum was deposited at the mineralization front (the interface between unmineralized and mineralizing bone matrix). This dense aluminum deposit could readily be demonstrated by electron microprobe and ion microscopy (18). Aluminum retards *de novo* bone mineral formation as well as the maturation of bone mineral (19–22). These unique properties of aluminum may explain the disordered and delayed mineralization of bone (aluminum-induced osteomalacia) that occurs following aluminum administration (23). The lower levels of gallium that accumulate in bone as well as the difference in its sites of accumulation clearly distinguish gallium from aluminum. Such differences may account for their separate biological effects on bone metabolism.

Treatment with gallium blocks bone resorption (1–6), causes an increase in bone calcium and phosphorus content, as well as an increase in size/or perfection of hydroxyapatite crystallites of maturing bone (11, 12). Therefore, it would appear that the interaction of gallium with bone is a favorable one, since bone destruction is inhibited and mineral accretion is enhanced. It is evident from the XRM data that gallium localizes to the regions of bone where these changes are affected and suggests that gallium acts locally to enhance osteoblast function and decrease osteoclastic activity. The changes in other trace elements (iron and zinc) that are associated with gallium treatment may provide an important clue as to the molecular targets (e.g., enzymes) for gallium. As the spatial resolution of synchrotron x-ray microscopy improves, further insights into the specific bone cells and subcellular targets affected by gallium will become evident.

This work was supported in part by Public Health Service Grants CA38645, CA42445, and CA29502 and National Institutes of Health Biotechnology Research Resource Grant P41RR01838. Development of the analytical instrumentation was supported by The U.S. Department of Energy, Office of Basic Energy Sciences, Division of Chemical Sciences, Processes and Techniques Branch, under contract DE-AC02-76CH00016.

1. Warrell, R. P., Jr., Bockman, R. S., Coonley, C. J., Isaacs, M. & Staszewski, H. J. (1984) *J. Clin. Invest.* **73,** 1487–1490.
2. Warrell, R. P., Jr., Isaacs, M., Coonley, C. J., Alcock, N. W. & Bockman, R. S. (1985) *Cancer Treat. Rep.* **69,** 653–655.
3. Warrell, R. P., Jr., Skelos, A., Alcock, N. W. & Bockman, R. S. (1986) *Cancer Res.* **46,** 4208–4212.
4. Warrell, R. P., Jr., Alcock, N. W. & Bockman, R. S. (1987) *J. Clin. Oncol.* **5,** 292–298.
5. Warrell, R. P., Jr., Isaacs, M., Alcock, N. W. & Bockman, R. S. (1987) *Ann. Intern. Med.* **107,** 683–686.
6. Warrell, R. P., Jr., Israel, R., Frisone, M., Snyder, T., Gaynor, J. J. & Bockman, R. S. (1988) *Ann. Intern. Med.* **108,** 669–674.
7. Cournot-Witmer, G., Plachot, J. J., Bourdeau, A., Lieberherr, M. & Balsan, S. (1986) *J. Bone Miner. Res.* **1,** 106.
8. Boskey, A. L., Bockman, R. S., Alcock, N., Repo, M. A., Betts, F., Blumenthal, N. C., Bansal, M. & Warrell, R. P., Jr. (1987) *Trans. Ann. Meet. Orthop. Res. Soc.* **12,** 170.
9. Dudley, H. C. & Maddox, G. E. (1949) *J. Pharmacol. Exp. Ther.* **96,** 224.
10. Anghileri, L. (1971) *Strahlentherapie* **142,** 456–462.
11. Bockman, R. S., Boskey, A. L., Blumenthal, N. C., Alcock, N. W. & Warrell, R. P., Jr. (1986) *Calcif. Tissue Int.* **39,** 376–381.
12. Repo, M. A., Bockman, R. S., Betts, F., Boskey, A. L. & Warrell, R. P., Jr. (1988) *Calcif. Tissue Int.* **43,** 300–306.
13. Mills, B. G., Masuoka, L. S., Graham, C. C., Singer, F. R. & Waxman, A. D. (1988) *J. Nucl. Med.* **29,** 1083–1087.
14. Jones, K. W., Gordon, B. M., Hanson, A. L., Pounds, J. G., Rivers, M. L. & Schidlovsky, G. (1985) *EMSA Bull.* **15,** 28–29.
15. Hanson, A. L., Jones, K. W., Gordon, B. M., Pounds, J. G., Kwiatek, W. M., Long, G. J., Rivers, M. L. & Sutton, S. R. (1987) *Nucl. Instrum. Methods* **25,** 400–404.
16. Jones, K. W., Gordon, B. M., Hanson, A. L., Kwiatek, W. M. & Pounds, J. G. (1988) *Ultramicroscopy* **24,** 313–328.
17. Kimmel, D. B. & Jee, W. S. S. (1980) *Calcif. Tissue Int.* **32,** 113–122.
18. Cournot-Witmer, G., Zingraff, J., Plachot, J. J., Escaig, F., Lefevre, R., Bonmati, P., Bourdeau, A., Grabedian, M., Galle, P., Bourdon, R., Drueke, T. & Balsan, S. (1981) *Kidney Int.* **20,** 375–385.
19. Hodsman, A. B., Sherrard, D. J., Alfrey, A. C., Ott, S., Brickman, A. S., Miller, M. L., Maloney, N. A. & Coburn, J. W. (1982) *J. Clin. Endocrinol. Metab.* **54,** 539–546.
20. Blumenthal, N. D. & Posner, A. S. (1984) *Calcif. Tissue Int.* **36,** 439–441.
21. Posner, A. S., Blumenthal, N. C. & Boskey, A. L. (1986) *Kidney Int.* **29,** S17–S19.
22. Ikeda, K., Matsumoto, T., Morita, M., Kurokawa, K. & Ogata, E. (1986) *Calcif. Tissue Int.* **39,** 319–323.
23. Clarkson, E. M., Luck, U. A., Hynson, W. V., Bailey, R. R., Eastwood, J. B., Woodhead, J. S., Clements, V. R., O'Riordan, J. L. & DeWardener, H. E. (1972) *Clin. Sci.* **43,** 519–531.